Air–Liquid Interfacial Self-Assembly of Conjugated Block Copolymers into Ordered Nanowire Arrays

Ma. Helen M. Cativo,[†] David K. Kim,[‡] Robert A. Riggleman,[§] Kevin G. Yager,[⊥] Stephen S. Nonnenmann,[‡,#] Huikuan Chao,[§] Dawn A. Bonnell,[‡] Charles T. Black,[⊥] Cherie R. Kagan,[†,‡,∥] and So-Jung Park*[,†,⊗]

[†]Departments of Chemistry, [‡]Materials Science and Engineering, [§]Chemical and Biomolecular Engineering, and [∥]Electrical and Systems Engineering, University of Pennsylvania, 231 South 34th Street, Philadelphia, Pennsylvania 19104, United States, [⊥]Center for Functional Nanomaterials, Brookhaven National Laboratory, Upton, New York 11973, United States, and [⊗]Department of Chemistry and Nano Science, Ewha Womans University, 52 Ewhayeodae-gil, Seodaemun-gu, Seoul, 120-750, Korea. [#]Present address: Department of Mechanical & Industrial Engineering, University of Massachusetts Amherst, Amherst, Massachusetts 01003, United States.

ABSTRACT The ability to control the molecular packing and nanoscale morphology of conjugated polymers is important for many of their applications. Here, we report the fabrication of well-ordered nanoarrays of conjugated polymers, based on the self-assembly of conjugated block copolymers at the air–liquid interface. We demonstrate that the self-assembly of poly(3-hexylthiophene)-*block*-poly(ethylene glycol) (P3HT-*b*-PEG) at the air–water interface leads to large-area free-standing films of well-aligned P3HT nanowires. Block copolymers with high P3HT contents (82–91%) formed well-ordered nanoarrays at the interface. The fluidic nature of the interface, block copolymer architecture, and rigid nature of P3HT were necessary for the formation of well-ordered nanostructures. The free-standing films formed at the interface can be readily transferred to arbitrary solid substrates. The P3HT-*b*-PEG films are integrated in field-effect transistors and show orders of magnitude higher charge carrier mobility than spin-cast films, demonstrating that the air–liquid interfacial self-assembly is an effective thin film fabrication tool for conjugated block copolymers.

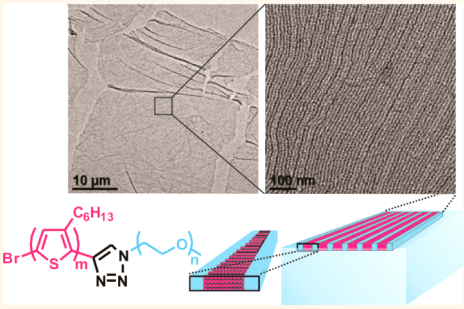

KEYWORDS: amphiphilic polymer · conjugated copolymer · air–water interface · self-assembly · supramolecular chemistry

The self-assembly of block copolymers has attracted significant attention for the past few decades, as it offers an attractive bottom-up alternative to traditional top-down patterning technologies.[1,2] While a majority of research in this area has been carried out with coil–coil-type polymers, there has been increasing interest in incorporating rod-type functional polymers (*e.g.*, conjugated polymers, polypeptides, DNA) into a block copolymer architecture.[3–5] The self-assembly of conjugated block copolymers is particularly interesting, as it can potentially generate conducting nanoarrays that can be integrated into organic electronic devices,[6–9] without additional pattern transfer or functionalization steps.

However, the self-assembly behavior of rod–coil-type conjugated block copolymers[10] is more complicated than widely studied, classical coil–coil-type polymers due to the rigidity and high melting temperature of conjugated polymers. For example, poly(3-hexylthiophene) (P3HT), which is one of the most widely used conjugated polymers,[11] has a melting temperature[12] of ~170–230 °C and a strong tendency to crystallize. Therefore, it is challenging to access equilibrium assembly structures of P3HT block copolymers with long-range order.[13–17] McCullough and co-workers first showed that P3HT block copolymers form locally ordered short nanofibrils in drop-cast films.[18] In a later study, they found that reducing the bulkiness of the coil block improved the ordering in drop-cast films of P3HT block copolymers with 17 wt % P3HT.[19] Dai and co-workers have demonstrated that ordered assemblies of P3HT block copolymers can be formed through thermal annealing when P3HT block content was less than 70 wt %.[13] Segalman and co-workers have recently shown that replacing the straight hexyl side chain of P3HT with a branched side chain of

* Address correspondence to sojungpark@ewha.ac.kr.

Received for review October 15, 2014 and accepted December 8, 2014.

Published online December 08, 2014
10.1021/nn505871b

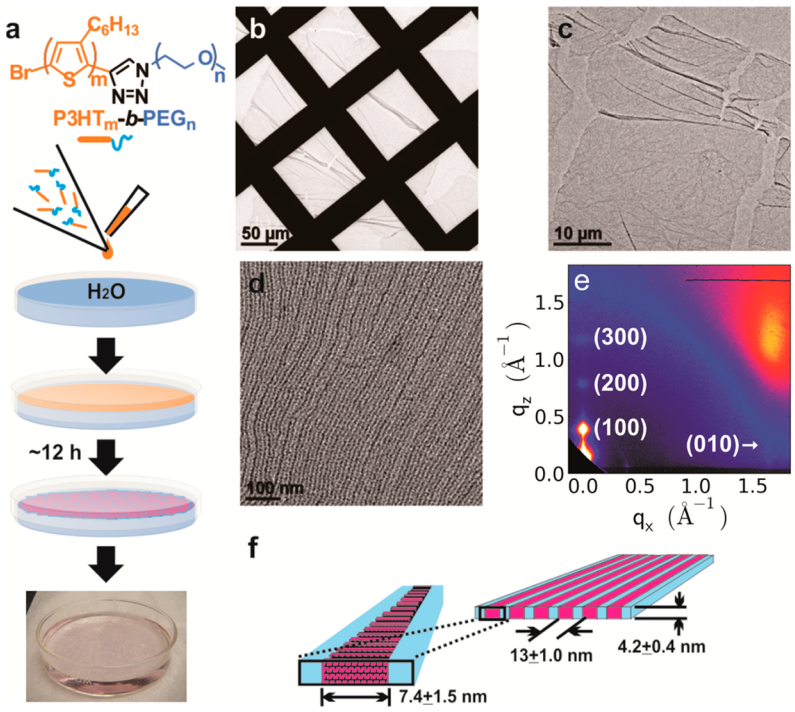

Figure 1. Self-assembly procedure and film characterization. (a) Schematic description for the self-assembly of P3HT-*b*-PEG at the air−water interface. (b−d) TEM images at different magnifications, (e) GIWAXS pattern, and (f) structural model of P3HT-*b*-PEG films fabricated by ALISA.

3-(2′-ethyl)hexylthiophene facilitates the formation of ordered polythiophene arrays.[20] However, the introduction of branched or long side chains on polythiophenes or of high molecular weight insulating blocks can negatively impact transport properties.[21]

Here, we report that the air−liquid interfacial self-assembly (ALISA) of P3HT diblock copolymers can lead to well-aligned P3HT nanowire arrays. Centimeter-scale, uniform, and continuous free-standing films of aligned P3HT nanowires were formed from block copolymers with high P3HT content (82−91 wt %) using this approach. The ability to control the nanoscale morphology and molecular packing structure of conjugated polymers is important for many of their applications.[22,23] The P3HT-*b*-PEG films formed by ALISA showed orders of magnitude higher current than disordered films of similar thickness when integrated into field-effect transistors (FETs) as semiconducting channels. We believe that this approach opens a new route for fabricating molecularly thin films of technologically important rod-type polymers with controlled nanoscale morphologies.

RESULTS AND DISCUSSION

Self-Assembly of P3HT-*b*-PEG at the Air−Water Interface. Diblock copolymers of poly(3-hexylthiophene)-*block*-poly(ethylene glycol) (P3HT-*b*-PEG) with regioregular P3HT blocks were synthesized by click chemistry following a previously reported procedure.[24] (See Supporting Information Figures S1 to S6 for characterization data.) In a typical self-assembly procedure, P3HT-*b*-PEG (4025 g/mol, 82 wt % P3HT) was first dissolved at 58 μM in toluene. A droplet (2.9 nmol, 50 μL) of the solution was gently placed on the water surface (Figure 1a) in a plastic tube. The tube was then capped and left undisturbed overnight to allow for slow evaporation of toluene. After the toluene evaporated, a pink film was observed on the water surface (Figure 1a) with areas ranging from 20 to 300 cm^2 depending on the container size. A detailed description of the procedure is provided in the Methods section. The film on the water surface was transferred onto various substrates for characterization and device integration by dipping the substrate into the water subphase.

Transmission electron microscope (TEM) images (Figure 1b,c and Supporting Information Figure S7) and additional characterization data (Supporting Information Figures S8 and S9) showed that large-area, continuous polymer films with uniform thickness were formed by ALISA without applying mechanical pressure. Higher magnification TEM images revealed that the films are composed of a periodic line pattern of P3HT-*b*-PEG (Figure 1d) with a periodicity of 13 ± 1.0 nm (see Supporting Information Figure S10 for the Fourier transform analysis of images). The amount of polymer placed at the interface was adjusted to obtain well-aligned assembly structures (Supporting Information Figure S11). The average ordered domain size was 1.7 ± 3.5 μm^2, with some domains reaching over 10 μm^2. The P3HT wire width (dark region of the TEM image) was measured to be 7.4 ± 1.5 nm, which

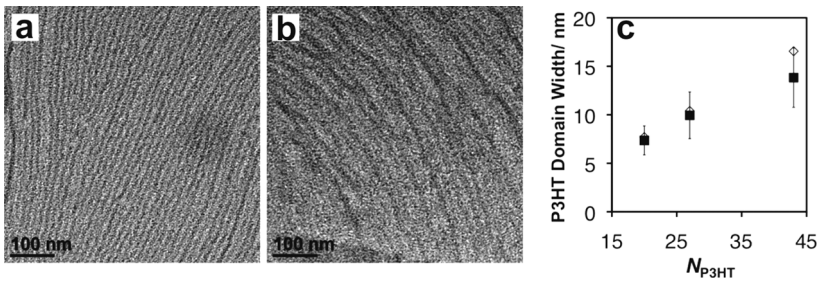

Figure 2. Self-assembly of block copolymers with different P3HT block lengths. (a, b) TEM images of P3HT-*b*-PEG nanowire arrays formed from (a) P3HT-*b*-PEG (5187 g/mol, 86 wt % P3HT) and (b) P3HT-*b*-PEG (7844 g/mol, 91 wt % P3HT). The degree of polymerization for P3HT (N_{P3HT}) was 27 (a) and 43 (b), respectively. (c) Measured P3HT domain width (closed squares) in P3HT-*b*-PEG nanoarrays. Open diamonds correspond to the calculated contour length (*aN*) of P3HT.

closely matches the length of fully extended P3HT[25] (7.7 nm) (see Supporting Information discussion). The alternating P3HT and PEG domains were also confirmed by staining PEG domains with phosphotungstic acid (Supporting Information Figure S7, k,l). Grazing incidence X-ray scattering (GIXS) (Figure 1e) of thin films transferred to a silicon wafer showed (*n*00) peaks with an interlayer distance of 16.2 Å along the thickness of the film (*z* direction) and a $\pi-\pi$ stacking distance of 3.8 Å along the plane of the film. The strong (*n*00) peaks along the *z* direction (Figure 1e and Supporting Information Figure S12) indicate that P3HT strands are stacked with an edge-on conformation. The film thickness was measured to be 4.2 $\pm$ 0.4 nm by atomic force microscopy (AFM) (Figure S8b), which corresponds to about three P3HT layers for the edge-on conformation. The structure of the self-assembled film constructed from the characterization data is illustrated in Figure 1f.

Polythiophene block copolymers with longer P3HT blocks, P3HT-*b*-PEG (5187 g/mol, 86 wt % P3HT) and P3HT-*b*-PEG (7844 g/mol, 91 wt % P3HT), showed similar assembly behavior, forming aligned nanowire arrays with different P3HT domain widths (Figure 2a,b). The P3HT widths measured from TEM images were plotted in Figure 2c along with the calculated contour lengths (*aN*) of P3HT, where *a* is the rod segment length[25] equal to 0.385 nm and *N* is the degree of polymerization. Overall, the measured widths were close to the calculated contour lengths, although slight deviations were observed for higher molecular weight polymers. This result shows that the aligned wire morphology is maintained at the higher P3HT content, and the P3HT domain size can be controlled by varying the length of polymer chains. Note that in previous bulk or thin-film studies of polyalkylthiophene block copolymers, a relatively long coil-type insulating block was necessary to form ordered structures.[13−15] In the air−liquid interfacial assembly reported here, on the other hand, ordered nanoarrays were formed from polymers with high P3HT contents (~91 wt % P3HT). In fact, a short insulating block is expected to be more favorable for the formation of nanowire arrays because long PEG strands can sterically hinder the elongation[24] of nanowires. Note that block copolymers with high P3HT wt % are advantageous for applications in organic electronics.

Mechanism of the Air−Liquid Interfacial Self-Assembly. Figure 3a−d shows TEM images of sample aliquots taken at different time intervals to monitor the progress of the self-assembly of P3HT-*b*-PEG at the air−water interface. During the first 5 min, short nanowires of P3HT-*b*-PEG started to form (Figure 3a). The nanowires began to bundle up within the first hour (Figure 3b), and then they grew into ordered nanowire arrays from 6 to 12 hours (Figure 3c,d). Overall, the aspect ratio of nanowires and the packing density increased over time as they packed and aligned into extended nanowire arrays. Figure 3e shows our proposed mechanism for the self-assembly. The primary structure of P3HT-*b*-PEG possesses the structural (rigidity) and chemical (π-stacking, alkyl chain packing, immiscibility between the two blocks) information necessary for the development of the secondary structure of nanowires:[24] the rigidity of the P3HT block drives rod−rod alignment,[26−28] and anisotropic interactions of $\pi-\pi$ stacking and alkyl side chain packing[29] lead to the formation of one-dimensional wires.[30,31] The secondary structure of nanowires in turn possesses structural (long aspect ratio, rigidity) and chemical (wetting) information that leads to the tertiary structure of two-dimensional nanowire arrays. The development of nanowire arrays is consistent with the Onsager theory,[32] which predicts entropy-driven alignment of anisotropic rod-shaped objects. The rigidity of P3HT-*b*-PEG nanowires was found to facilitate their alignment. In our control experiments, the air−water interfacial self-assembly of P3HT-*b*-PEG was sensitive to the oxidation of P3HT, and the typical well-aligned nanowire arrays were not observed from the films of oxidized P3HT-*b*-PEG, which contains a relatively more flexible rod block than pristine P3HT-*b*-PEG (Supporting Information Figure S13).

The diblock structure of P3HT-*b*-PEG was also found to be important for the formation of well-ordered nanowire arrays. Control samples of P3HT homopolymers and a mixture of P3HT and PEG homopolymers

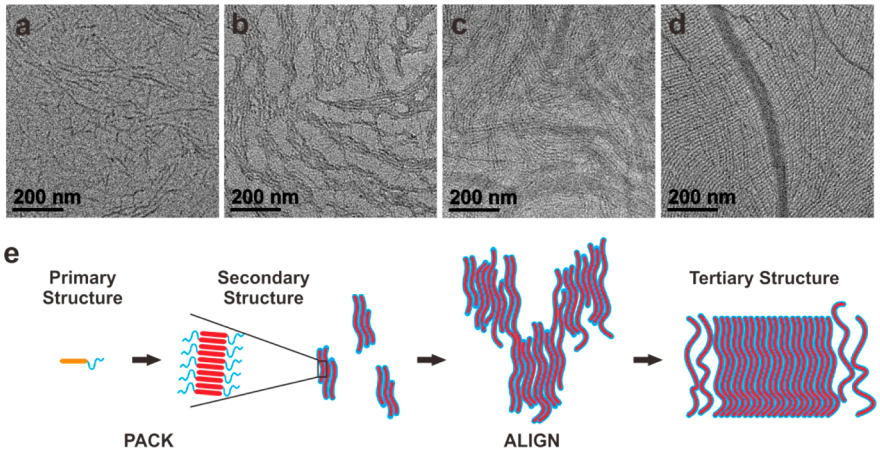

Figure 3. Mechanism of the air−liquid interfacial self-assembly (ALISA). (a−d) TEM images showing the time evolution of P3HT-*b*-PEG nanowire arrays at 5 min (a), 1 h (b), 6 h (c), and 12 h (d) (initial conditions: 100 μL of 30 μM P3HT-*b*-PEG in toluene). (e) Proposed mechanism for the formation of hierarchical P3HT-*b*-PEG nanowire arrays.

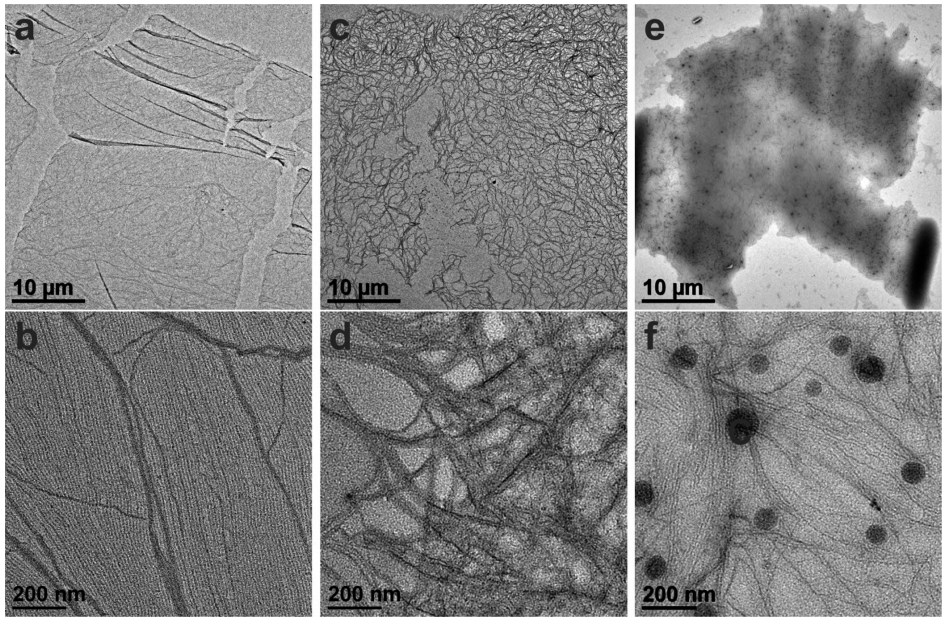

Figure 4. Effect of the diblock copolymer structure on the self-assembly. TEM images of films made from (a, b) P3HT-*b*-PEG, (c, d) P3HT only, and (e, f) a P3HT/PEG mixture.

did not form ordered arrays under the same conditions (Figure 4). Instead, P3HT homopolymers formed porous networks of entangled nanofibrils, and the mixture of P3HT and PEG homopolymers formed disordered fibers and spherical aggregates. In our self-assembly of P3HT-*b*-PEG, hydrophilic PEG chains surrounding the P3HT nanowires prevent the nanowires from entangling with each other. In addition, our control experiments for the self-assembly of P3HT-*b*-PEG on solid substrates (silicon wafer, glass) generated disordered films (Supporting Information Figures S14 and S15), indicating that the mobility of the fluid interface is important for the formation of well-ordered structures. The slow evaporation of toluene was another important factor for the formation of well-aligned nanowire arrays (Supporting Information Figure S16).

Coarse-Grained Simulations. Coarse-grained simulations (Figure 5 and Supporting Information Figure S17) were performed on a model rod−coil block copolymer that was initially placed at the interface between model hydrophilic (coil-favoring) and hydrophobic (rod-favoring) solvents. The rigidity of the backbone of the rod block was varied from fully flexible (Figure 5a, $k_\theta = 0$, left) to semiflexible polymer (Figure 5a, $k_\theta = 10$, right), where the force constant k_θ dictates the strength of the potential that maintains the polymer backbone rigidity. In the long-chain limit, the persistence lengths for $k_\theta = 0$ and 10 are approximately 1σ and 10σ, respectively, where σ is the size of the monomer. Therefore, we are spanning the range from fully flexible polymers where the contour length is much larger than the persistence length to nearly rigid polymers, where the contour

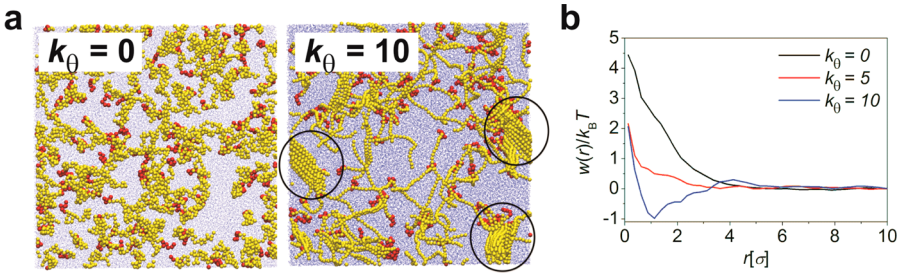

Figure 5. Coarse-grained simulations performed on a model rod−coil block copolymer. (a) Top-down view of coil−coil (k_θ = 0, left) and rod−coil diblock copolymers (k_θ = 10, right) at the fluid interface between hydrophobic (not shown) and hydrophilic (light blue) solvents captured at an early stage of self-assembly. P3HT and PEG blocks are colored yellow and red, respectively. (b) Potential of mean force, $w(r)/k_BT$, calculated between the centers of mass for polymers of varying stiffness k_θ.

length is only approximately 2.5 times the persistence length. At the early stage of solvent evaporation, ordering between the semiflexible blocks of the copolymers was observed (Figure 5a, right), which was absent in the fully flexible polymers (Figure 5a, left). This observation is consistent with the calculated potential of mean force between polymer strands (Figure 5b), where an attractive well was observed only for a rigid polymer (k_θ = 10). By separating the potential of mean force into its entropic and energetic components, we found that the interchain repulsion in the flexible chains has an entropic origin. The configurational entropy of the flexible chains prevents them from aggregating into bundles, while the semiflexible chains have a reduced configurational entropy and are able to form bundles. The ordering and bundling of semiflexible rod−coil copolymers at the interface became more pronounced as the evaporation proceeded. Upon completion of the solvent evaporation, the semiflexible rod−coil copolymers formed an anisotropic aggregate with large domains where the semiflexible blocks are aligned parallel to each other [Supporting Information Figure S17a (left), b]. In contrast, the coil−coil block copolymers formed a spherical micelle that sits at the air/hydrophilic solvent interface [Supporting Information Figure S17a (right), b]. These changes in the aggregate shape were quantified by calculating and diagonalizing the moment of inertia tensor; from its eigenvalues, we calculate the asphericity (α), which is only zero when the three principle moments are identical, as for a sphere. We find that α = 0.03, 0.52, and 0.94 for k_θ = 0, 5, and 10, respectively. Our simulation for the second step of the self-assembly (*i.e.*, nanowire alignment) using a highly coarse-grained model (Supporting Information Figure S18) showed that the rigidity of nanowires also plays a key role in the nanowire alignment.

Electrical Transport Measurements. To probe the transport properties of P3HT-*b*-PEG films fabricated by ALISA, the free-standing films formed from P3HT-*b*-PEG with 82 wt % P3HT (80 vol % P3HT) were integrated as the semiconductor channels in FETs. Prefabricated gold electrodes on a thermally oxidized, highly doped silicon wafer were dipped through the air−water interface to transfer the film and form the channel. The electrodes, thermally grown oxide layer, and the n-doped silicon served as source and drain, gate dielectric layer, and gate electrode, respectively. As presented in Figure 6, the films fabricated by ALISA behaved as a typical p-type semiconductor, seen as the negative gate bias (V_G) increases the hole concentration contributing to the drain current (I_D) (Figure 6a,b). The current level of the ALISA film was orders of magnitude higher than those of spin-cast films of comparable thickness (Figure 6b,c) owing to the well-ordered packing structure and desirable nanowire morphology of ALISA films. The measured hole mobility of ALISA films shows slight channel length dependence (Figure 6c,d) due to the micrometer-scale domain size. Nonetheless, the hole mobilities of the film (4−10 nm in thickness) were found to be 1 to 2 orders of magnitude higher than thicker (100 nm) films from similar molecular weight P3HT.[33,34] This result demonstrates that the ALISA of conjugated block copolymers is an effective thin-film fabrication method especially for very thin films (<20 nm) of conjugated polymers. In FETs, current modulation happens only within a very thin layer (*i.e.*, effective Debye length of two to five monolayers[35]) at the semiconductor/dielectric interface; thus thick films are not necessary as shown by previous reports on self-assembled monolayer transistors.[36−38] In fact, the structure of the bulk of the film is not necessarily reflective of the most important layer at the interface,[39] which makes the correlation of the structure and properties difficult. The well-defined morphology of the molecularly thin films formed by ALISA provides a means to systematically study structure−property relationships of conjugated polymer films integrated in organic FETs.

CONCLUSION

In summary, we demonstrated that uniform free-standing films composed of well-aligned P3HT nanowires can be readily constructed by the air−liquid interfacial self-assembly of P3HT block copolymers. This approach is applicable to other conjugated block copolymers in addition to P3HT block copolymers studied here. For example, air−liquid interfacial assembly of a relevant polymer, poly[3-(2,5,8,11-tetraoxatridecanyl)thiophene]-*block*-poly(ethylene glycol)

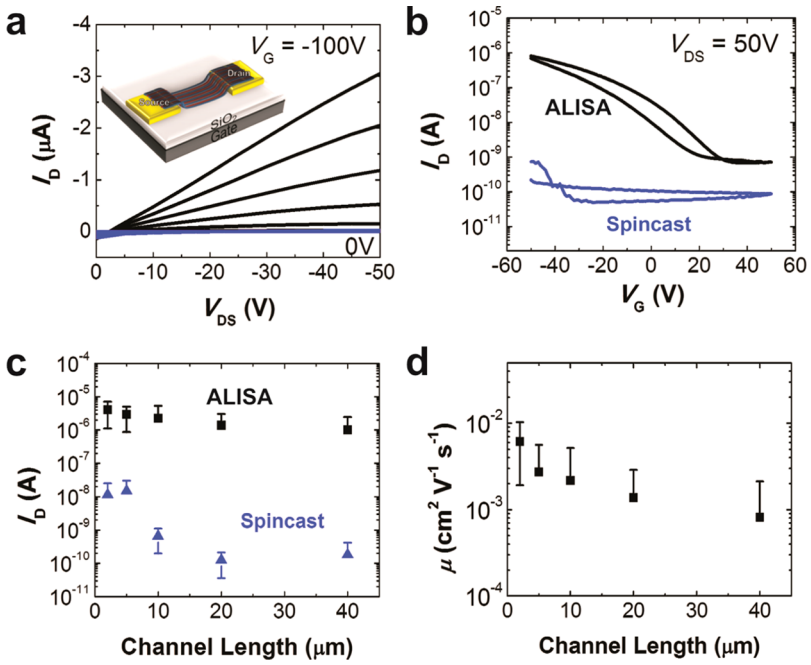

Figure 6. FET characteristics of P3HT-*b*-PEG films. Polymer films were prepared by ALISA (black curve or squares) or spin-casting (blue curve or triangles). (a) Output I_D-V_{DS}, (b) transfer I_D-V_G characteristics for a channel length of 10 μm in the saturation regime, and (c) channel length dependence of on-currents. (d) Hole mobilities for P3HT-*b*-PEG FETs fabricated by ALISA.

(PTOTT-*b*-PEG)[40] resulted in the formation of uniform two-dimensional sheets with a distinct packing structure (Supporting Information Figure S19). Researchers have previously shown that the conformation of conjugated homopolymers can be controlled by the Langmuir–Blodgett (LB) technique.[41–43] The LB technique has also been applied in the formation of a polymer nanostrand network from coil–coil-type block copolymers.[44–47] Here, we demonstrated that air–liquid interfacial assembly of conjugated block copolymers can be used to obtain thin films of functional polymers with controlled nanoscale morphology as well as the molecular packing and conformation. The fluidic nature of the air–water interface, rigid nature of the rod block, and the block copolymer architecture were found to be important for the formation of well-aligned nanowire arrays. When integrated into FET devices, P3HT-*b*-PEG films fabricated by ALISA showed orders of magnitude higher current than those prepared by conventional spin-coating, which demonstrates that the air–liquid interfacial self-assembly provides an excellent tool for fabricating molecularly thin conducting polymer films. The fluidic interfacial self-assembly has been actively used for ordering microscale and nanoscale objects[48–52] in recent years. We believe that the self-assembly at fluidic interfaces is especially useful for conjugated block copolymers, as it allows for the fabrication of well-defined ordered assembly structures that are difficult to access by conventional techniques due to the deep trapping of kinetic structures.

METHODS

Preparation of P3HT-*b*-PEG Film by ALISA. In a typical self-assembly, P3HT-*b*-PEG (4025 g/mol, 82 wt % P3HT) was dissolved in toluene and filtered with a 0.45 μm PTFE filter to prepare a stock solution of P3HT-*b*-PEG. The concentration of the stock solution was determined from the absorption spectrum with the measured extinction coefficient of P3HT-*b*-PEG ($\sim$1.0 $\times$ 10^5 M^{-1} cm^{-1}). A 30 μM solution was subsequently prepared from the stock solution. The solution was immediately used for the preparation of the film. A 100 μL aliquot of the 30 μM solution was then gently placed in direct contact with the water surface where the water is contained inside a 2.7 cm diameter 50 mL polypropylene centrifuge tube. The tube was immediately capped loosely, and toluene was left to evaporate slowly overnight. Alternatively, a 100 μL aliquot of a 100 μM solution was placed over water in a covered 10 cm diameter glass Petri dish, and toluene was left to evaporate slowly overnight. Detailed methods on the synthesis, film characterization, and analysis are available in the Supporting Information.

Coarse-Grained Simulations. Our coarse-grained molecular dynamics simulations consist of an A–B diblock copolymer modeled using a modified version of the canonical Kremer–Grest model[53] placed at the interface between an A solvent and a B solvent. The attractive energy of interaction between all like monomers was set to $\varepsilon = 5/3\ k_BT$, while cross interactions had a reduced value of 0.5ε to force phase separation between the dissimilar components. A bending potential with strength k_θ was added to the hydrophobic (B) block to investigate the effect of the rigidity on the interfacial self-assembly. Evaporation of the hydrophobic solvent was mimicked by alternately selecting at random and removing a portion of the hydrophobic solvent and re-equilibrating the system with a reduced solvent content.

Complete details of the model parameters, equilibration protocol, and analysis are given in the Supporting Information.

Transport Measurement. Devices were fabricated on highly n-doped Si wafers (ρ < 0.01 Ω-cm) with 250 nm thermally grown SiO_2 from Silicon Quest. Electrodes were patterned photolithographically, utilizing a bilayer of Lift-off Resist (LOR3A from MicroChem) and S1814 (Microposit) to define channel lengths between 2 and 40 μm with a channel width to channel length (W/L) ratio of 20. The samples were cleaned by a 3 min O_2 plasma prior to metal deposition by thermal evaporation of 2 nm Ti and 18 nm Au. Metal was subsequently lifted off using Remover PG (MicroChem). Fabricated devices were cleaned with chloroform and acetone and then placed in a UV-ozone cleaner for 30 min. Right after UV-ozone cleaning, devices were placed in a vacuum desiccator at room temperature with 2.0 mL of hexamethyldisilazane (HMDS, Aldrich, 99.9%), then pumped down to pressures below 1 Torr to vapor prime the SiO_2 surface with HMDS. Samples were then ready for nanowire deposition. The nanowire film was prepared at the air−water interface as described above. Devices were vertically dipped into the air−water interface to transfer the film onto the device, followed by removal of the remaining film at the interface to prevent multilayer deposition.

Device characterization was performed on an Agilent 4156C semiconductor parameter analyzer in combination with a Karl Suss PM5 probe station mounted in a nitrogen glovebox. The devices operate in accumulation mode upon application of a negative gate bias as the concentration of majority carrier holes contributing to I_D increases. Device operation was modeled by standard FET equations in saturation:

$$\mu_{SAT} = \frac{2L}{C_{DEL}W}\left(\frac{\partial I_D}{\partial V_G}\right)^2$$

where L is the channel length, W is the channel width, C_{DIEL} is the capacitance per unit area of the dielectric layer, and the square-root of the current I_D rises linearly with V_G and can be used to extract the transconductance in the saturation regime. Transconductance values were consistently extrapolated from the forward sweep (negative to positive).

Conflict of Interest: The authors declare no competing financial interest.

Supporting Information Available: Detailed synthesis and characterization of P3HT-*b*-PEG, calculation of expected P3HT domain size, additional characterization of P3HT-*b*-PEG films (TEM, scanning electron microscopy, AFM, optical microscopy, confocal microscopy, UV−vis spectroscopy, conductive AFM, GIXS), additional data for the self-assembly of P3HT-*b*-PEG, additional coarse-grained simulations. This material is available free of charge *via* the Internet at http://pubs.acs.org.

Acknowledgment. This work was supported by the ARO Young Investigator Award (W911NF-09-1-0146), the Agency for Defense Development, South Korea, and the Nano/Bio Interface Center through the National Science Foundation (NSF) NSEC DMR08-32802. D.K.K. and C.R.K. acknowledge support from NSF under Award CBET-1236406. The authors thank Yuming Lai and Scott Stinner for additional help in the electrical measurements. Use of University of Pennsylvania Nano/Bio Interface Center instrumentation is acknowledged.

REFERENCES AND NOTES

1. Bates, F. S.; Fredrickson, G. H. Block Copolymer Thermodynamics: Theory and Experiment. *Annu. Rev. Phys. Chem.* **1990**, *41*, 525–557.
2. Lodge, T. P. Block Copolymers: Past Successes and Future Challenges. *Macromol. Chem. Phys.* **2003**, *204*, 265–273.
3. Yassar, A.; Miozzo, L.; Gironda, R.; Horowitz, G. Rod−Coil and All-Conjugated Block Copolymers for Photovoltaic Applications. *Prog. Polym. Sci.* **2013**, *38*, 791–844.
4. Zhang, J.; Chen, X.-F.; Wei, H.-B.; Wan, X.-H. Tunable Assembly of Amphiphilic Rod-Coil Block Copolymers in Solution. *Chem. Soc. Rev.* **2013**, *42*, 9127–9154.
5. Kim, H. J.; Kim, J.-H.; Ryu, J.-H.; Kim, Y.; Kang, H.; Lee, W. B.; Kim, T.-S.; Kim, B. J. Architectural Engineering of Rod−Coil Compatibilizers for Producing Mechanically and Thermally Stable Polymer Solar Cells. *ACS Nano* **2014**, *8*, 10461–10470.
6. Javier, A. E.; Patel, S. N.; Hallinan, D. T.; Srinivasan, V.; Balsara, N. P. Simultaneous Electronic and Ionic Conduction in a Block Copolymer: Application in Lithium Battery Electrodes. *Angew. Chem., Int. Ed.* **2011**, *50*, 9848–9851.
7. Patel, S. N.; Javier, A. E.; Stone, G. M.; Mullin, S. A.; Balsara, N. P. Simultaneous Conduction of Electronic Charge and Lithium Ions in Block Copolymers. *ACS Nano* **2012**, *6*, 1589–1600.
8. Patel, S. N.; Javier, A. E.; Balsara, N. P. Electrochemically Oxidized Electronic and Ionic Conducting Nanostructured Block Copolymers for Lithium Battery Electrodes. *ACS Nano* **2013**, *7*, 6056–6068.
9. Patel, S. N.; Javier, A. E.; Beers, K. M.; Pople, J. A.; Ho, V.; Segalman, R. A.; Balsara, N. P. Morphology and Thermodynamic Properties of a Copolymer with an Electronically Conducting Block: Poly(3-Ethylhexylthiophene)-Block-Poly(Ethylene Oxide). *Nano Lett.* **2012**, *12*, 4901–4906.
10. Olsen, B. D.; Segalman, R. A. Self-Assembly of Rod−Coil Block Copolymers. *Mater. Sci. Eng., R* **2008**, *62*, 37–66.
11. Sirringhaus, H.; Brown, P. J.; Friend, R. H.; Nielsen, M. M.; Bechgaard, K.; Langeveld-Voss, B. M. W.; Spiering, A. J. H.; Janssen, R. A. J.; Meijer, E. W.; Herwig, P.; *et al*. Two-Dimensional Charge Transport in Self-Organized, High-Mobility Conjugated Polymers. *Nature* **1999**, *401*, 685–688.
12. Zen, A.; Saphiannikova, M.; Neher, D.; Grenzer, J.; Grigorian, S.; Pietsch, U.; Asawapirom, U.; Janietz, S.; Scherf, U.; Lieberwirth, I.; *et al*. Effect of Molecular Weight on the Structure and Crystallinity of Poly(3-Hexylthiophene). *Macromolecules* **2006**, *39*, 2162–2171.
13. Dai, C.-A.; Yen, W.-C.; Lee, Y.-H.; Ho, C.-C.; Su, W.-F. Facile Synthesis of Well-Defined Block Copolymers Containing Regioregular Poly(3-Hexyl Thiophene) *via* Anionic Macroinitiation Method and Their Self-Assembly Behavior. *J. Am. Chem. Soc.* **2007**, *129*, 11036–11038.
14. Moon, H. C.; Bae, D.; Kim, J. K. Self-Assembly of Poly(3-Dodecylthiophene)-*Block*-Poly(Methyl Methacrylate) Copolymers Driven by Competition between Microphase Separation and Crystallization. *Macromolecules* **2012**, *45*, 5201–5207.
15. Kim, H. J.; Paek, K.; Yang, H.; Cho, C.-H.; Kim, J.-S.; Lee, W.; Kim, B. J. Molecular Design of "Graft" Assembly for Ordered Microphase Separation of P3HT-Based Rod−Coil Copolymers. *Macromolecules* **2013**, *46*, 8472–8478.
16. Lee, Y.-H.; Yen, W.-C.; Su, W.-F.; Dai, C.-A. Self-Assembly and Phase Transformations of π-Conjugated Block Copolymers That Bend and Twist: From Rigid-Rod Nanowires to Highly Curvaceous Gyroids. *Soft Matter* **2011**, *7*, 10429–10442.
17. Yu, X.; Xiao, K.; Chen, J.; Lavrik, N. V.; Hong, K.; Sumpter, B. G.; Geohegan, D. B. High-Performance Field-Effect Transistors Based on Polystyrene-B-Poly(3-Hexylthiophene) Diblock Copolymers. *ACS Nano* **2011**, *5*, 3559–3567.
18. Liu, J. S.; Sheina, E.; Kowalewski, T.; McCullough, R. D. Tuning the Electrical Conductivity and Self-Assembly of Regioregular Polythiophene by Block Copolymerization: Nanowire Morphologies in New Di- and Triblock Copolymers. *Angew. Chem., Int. Ed.* **2002**, *41*, 329–332.
19. Iovu, M. C.; Zhang, R.; Cooper, J. R.; Smilgies, D. M.; Javier, A. E.; Sheina, E. E.; Kowalewski, T.; McCullough, R. D. Conducting Block Copolymers of Regioregular Poly(3-Hexylthiophene) and Poly(Methacrylates): Electronic Materials with Variable Conductivities and Degrees of Interfibrillar Order. *Macromol. Rapid Commun.* **2007**, *28*, 1816–1824.
20. Ho, V.; Boudouris, B. W.; McCulloch, B. L.; Shuttle, C. G.; Burkhardt, M.; Chabinyc, M. L.; Segalman, R. A. Poly(3-Alkylthiophene) Diblock Copolymers with Ordered Microstructures and Continuous Semiconducting Pathways. *J. Am. Chem. Soc.* **2011**, *133*, 9270–9273.

21. Ho, V.; Boudouris, B. W.; Segalman, R. A. Tuning Polythiophene Crystallization through Systematic Side Chain Functionalization. *Macromolecules* **2010**, *43*, 7895–7899.
22. Gao, Y.; Grey, J. K. Resonance Chemical Imaging of Polythiophene/Fullerene Photovoltaic Thin Films: Mapping Morphology-Dependent Aggregated and Unaggregated C═C Species. *J. Am. Chem. Soc.* **2009**, *131*, 9654–9662.
23. Lee, S. S.; Loo, Y.-L. Structural Complexities in the Active Layers of Organic Electronics. *Annu. Rev. Chem. Biomol. Eng.* **2010**, *1*, 59–78.
24. Kamps, A. C.; Fryd, M.; Park, S.-J. Hierarchical Self-Assembly of Amphiphilic Semiconducting Polymers into Isolated, Bundled, and Branched Nanofibers. *ACS Nano* **2012**, *6*, 2844–2852.
25. Brinkmann, M.; Wittmann, J. C. Orientation of Regioregular Poly(3-Hexylthiophene) by Directional Solidification: A Simple Method to Reveal the Semicrystalline Structure of a Conjugated Polymer. *Adv. Mater.* **2006**, *18*, 860–863.
26. Pryamitsyn, V.; Ganesan, V. Self-Assembly of Rod−Coil Block Copolymers. *J. Chem. Phys.* **2004**, *120*, 5824–5838.
27. Tcherniak, A.; Solis, D.; Khatua, S.; Tangonan, A. A.; Lee, T. R.; Link, S. Chain-Length Dependent Nematic Ordering of Conjugated Polymers in a Liquid Crystal Solvent. *J. Am. Chem. Soc.* **2008**, *130*, 12262–12263.
28. Chung, W.-J.; Oh, J.-W.; Kwak, K.; Lee, B. Y.; Meyer, J.; Wang, E.; Hexemer, A.; Lee, S.-W. Biomimetic Self-Templating Supramolecular Structures. *Nature* **2011**, *478*, 364–368.
29. Liu, J.; Arif, M.; Zou, J.; Khondaker, S. I.; Zhai, L. Controlling Poly(3-Hexylthiophene) Crystal Dimension: Nanowhiskers and Nanoribbons. *Macromolecules* **2009**, *42*, 9390–9393.
30. Patra, S. K.; Ahmed, R.; Whittell, G. R.; Lunn, D. J.; Dunphy, E. L.; Winnik, M. A.; Manners, I. Cylindrical Micelles of Controlled Length with a π-Conjugated Polythiophene Core *via* Crystallization-Driven Self-Assembly. *J. Am. Chem. Soc.* **2011**, *133*, 8842–8845.
31. Qian, J.; Li, X.; Lunn, D. J.; Gwyther, J.; Hudson, Z. M.; Kynaston, E.; Rupar, P. A.; Winnik, M. A.; Manners, I. Uniform, High Aspect Ratio Fiber-Like Micelles and Block Co-Micelles with a Crystalline π-Conjugated Polythiophene Core by Self-Seeding. *J. Am. Chem. Soc.* **2014**, *136*, 4121–4124.
32. Onsager, L. The Effects of Shape on the Interaction of Colloidal Particles. *Ann. N.Y. Acad. Sci.* **1949**, *51*, 627–659.
33. Zhang, R.; Li, B.; Iovu, M. C.; Jeffries-El, M.; Sauvé, G.; Cooper, J.; Jia, S.; Tristram-Nagle, S.; Smilgies, D. M.; Lambeth, D. N.; *et al*. Nanostructure Dependence of Field-Effect Mobility in Regioregular Poly(3-Hexylthiophene) Thin Film Field Effect Transistors. *J. Am. Chem. Soc.* **2006**, *128*, 3480–3481.
34. Noriega, R.; Rivnay, J.; Vandewal, K.; Koch, F. P. V.; Stingelin, N.; Smith, P.; Toney, M. F.; Salleo, A. A General Relationship between Disorder, Aggregation and Charge Transport in Conjugated Polymers. *Nat. Mater.* **2013**, *12*, 1038–1044.
35. Shehu, A.; Quiroga, S. D.; D'Angelo, P.; Albonetti, C.; Borgatti, F.; Murgia, M.; Scorzoni, A.; Stoliar, P.; Biscarini, F. Layered Distribution of Charge Carriers in Organic Thin Film Transistors. *Phys. Rev. Lett.* **2010**, *104*, 246602.
36. Tulevski, G. S.; Miao, Q.; Fukuto, M.; Abram, R.; Ocko, B.; Pindak, R.; Steigerwald, M. L.; Kagan, C. R.; Nuckolls, C. Attaching Organic Semiconductors to Gate Oxides: *In Situ* Assembly of Monolayer Field Effect Transistors. *J. Am. Chem. Soc.* **2004**, *126*, 15048–15050.
37. Mathijssen, S. G. J.; Smits, E. C. P.; van Hal, P. A.; Wondergem, H. J.; Ponomarenko, S. A.; Moser, A.; Resel, R.; Bobbert, P. A.; Kemerink, M.; Janssen, R. A. J.; *et al*. Monolayer Coverage and Channel Length Set the Mobility in Self-Assembled Monolayer Field-Effect Transistors. *Nat. Nanotechnol.* **2009**, *4*, 674–680.
38. Kagan, C. R. Molecular Monolayers as Semiconducting Channels in Field Effect Transistors. In *Unimolecular and Supramolecular Electronics I*; Metzger, R. M., Ed.; Springer: Berlin, 2012; pp 213−237.
39. Koch, N. Organic Electronic Devices and Their Functional Interfaces. *ChemPhysChem* **2007**, *8*, 1438–1455.
40. Kamps, A. C.; Cativo, M. H. M.; Fryd, M.; Park, S.-J. Self-Assembly of Amphiphilic Conjugated Diblock Copolymers into One-Dimensional Nanoribbons. *Macromolecules* **2014**, *47*, 161–164.
41. Reitzel, N.; Greve, D. R.; Kjaer, K.; Howes, P. B.; Jayaraman, M.; Savoy, S.; McCullough, R. D.; McDevitt, J. T.; Bjørnholm, T. Self-Assembly of Conjugated Polymers at the Air/Water Interface. Structure and Properties of Langmuir and Langmuir-Blodgett Films of Amphiphilic Regioregular Polythiophenes. *J. Am. Chem. Soc.* **2000**, *122*, 5788–5800.
42. Kim, J.; Swager, T. M. Control of Conformational and Interpolymer Effects in Conjugated Polymers. *Nature* **2001**, *411*, 1030–1034.
43. Mattu, J. S.; Leach, G. W. Large Scale Crystallinity in Kinetically Stable Polythiophene-Based Langmuir-Blodgett Films. *J. Am. Chem. Soc.* **2010**, *132*, 3204–3210.
44. Devereaux, C. A.; Baker, S. M. Surface Features in Langmuir-Blodgett Monolayers of Predominantly Hydrophobic Poly(Styrene)-Poly(Ethylene Oxide) Diblock Copolymer. *Macromolecules* **2002**, *35*, 1921–1927.
45. Perepichka, I. I.; Badia, A.; Bazuin, C. G. Nanostrand Formation of Block Copolymers at the Air/Water Interface. *ACS Nano* **2010**, *4*, 6825–6835.
46. Cheyne, R. B.; Moffitt, M. G. Self-Assembly of Polystyrene-Block-Poly(Ethylene Oxide) Copolymers at the Air−Water Interface: Is Dewetting the Genesis of Surface Aggregate Formation? *Langmuir* **2006**, *22*, 8387–8396.
47. Cox, J. K.; Yu, K.; Constantine, B.; Eisenberg, A.; Lennox, R. B. Polystyrene−Poly(Ethylene Oxide) Diblock Copolymers Form Well-Defined Surface Aggregates at the Air/Water Interface. *Langmuir* **1999**, *15*, 7714–7718.
48. Dong, A.; Chen, J.; Vora, P. M.; Kikkawa, J. M.; Murray, C. B. Binary Nanocrystal Superlattice Membranes Self-Assembled at the Liquid-Air Interface. *Nature* **2010**, *466*, 474–477.
49. Niu, Z.; He, J.; Russell, T. P.; Wang, Q. Synthesis of Nano/Microstructures at Fluid Interfaces. *Angew. Chem., Int. Ed.* **2010**, *49*, 10052–10066.
50. Cavallaro, M.; Botto, L.; Lewandowski, E. P.; Wang, M.; Stebe, K. J. Curvature-Driven Capillary Migration and Assembly of Rod-Like Particles. *Proc. Natl. Acad. Sci. U.S. A.* **2011**, *108*, 20923–20928.
51. Park, J. Y.; Advincula, R. C. Nanostructuring Polymers, Colloids, and Nanomaterials at the Air-Water Interface through Langmuir and Langmuir-Blodgett Techniques. *Soft Matter* **2011**, *7*, 9829–9843.
52. Cui, M.; Emrick, T.; Russell, T. P. Stabilizing Liquid Drops in Nonequilibrium Shapes by the Interfacial Jamming of Nanoparticles. *Science* **2013**, *342*, 460–463.
53. Kremer, K.; Grest, G. S. Dynamics of Entangled Linear Polymer Melts: A Molecular-Dynamics Simulation. *J. Chem. Phys.* **1990**, *92*, 5057–5086.